

Emergent SU(4) Symmetry in α -ZrCl₃ and Crystalline Spin-Orbital Liquids

Masahiko G. Yamada,^{1,*} Masaki Oshikawa,¹ and George Jackeli^{2,3,†}

¹*Institute for Solid State Physics, University of Tokyo, Kashiwa 277-8581, Japan.*

²*Institute for Functional Matter and Quantum Technologies,*

University of Stuttgart, Pfaffenwaldring 57, D-70569 Stuttgart, Germany.

³*Max Planck Institute for Solid State Research, Heisenbergstrasse 1, D-70569 Stuttgart, Germany.*

(Dated: July 18, 2018)

While the enhancement of the spin-space symmetry from the usual SU(2) to SU(N) is promising for finding nontrivial quantum spin liquids, its realization in magnetic materials remains challenging. Here we propose a new mechanism by which the SU(4) symmetry emerges in the strong spin-orbit coupling limit. In d^1 transition metal compounds with edge-sharing anion octahedra, the spin-orbit coupling gives rise to strongly bond-dependent and apparently SU(4)-breaking hopping between the $J_{\text{eff}} = 3/2$ quartets. However, in the honeycomb structure, a gauge transformation maps the system to an SU(4)-symmetric Hubbard model. In the strong repulsion limit at quarter filling, as realized in α -ZrCl₃, the low-energy effective model is the SU(4) Heisenberg model on the honeycomb lattice, which cannot have a trivial gapped ground state and is expected to host a gapless spin-orbital liquid. By generalizing this model to other three-dimensional lattices, we also propose crystalline spin-orbital liquids protected by this emergent SU(4) symmetry and space group symmetries.

PhySH: Frustrated magnetism, Spin liquid, Quantum spin liquid

Introduction. — Nontrivial quantum spin liquids (QSLs) are expected to exhibit many exotic properties such as fractionalized excitations [1, 2], in addition to the absence of the long-range order. Despite the vigorous studies in the last several decades, however, material candidates for such QSLs are still rather limited.

An intriguing scenario to realize a nontrivial QSL is by generalizing the spin system, which usually consists of spins representing the SU(2) symmetry, to SU(N) “spin” systems with $N > 2$. We expect stronger quantum fluctuations in SU(N) spin systems with a larger N , which could lead the system to an SU(N) QSL even on unfrustrated, bipartite lattices, including the honeycomb lattice [3–6].

The SU(N) spin systems with $N > 2$ can be realized in ultracold atomic systems, using the nuclear spin degrees of freedom [7]. In electron spin systems, however, realization of this SU(N) symmetry is more challenging. It would be possible to combine the spin and orbital degrees of freedom, so that local electronic states are identified with a representation of SU(N). QSL realized in this context may be called quantum spin-orbital liquids (QSOLs) because it involves spin and orbital degrees of freedom. Despite the appeal of such a possibility, the actual Hamiltonian is usually not SU(N)-symmetric, reflecting the different physical origins of the spin and orbital degrees of freedom. For example, the relevance of an SU(4) QSOL has been discussed for Ba₃CuSb₂O₉ (BCSO) with a decorated honeycomb lattice structure [5, 8, 9]. It turned out, however, that the estimated parameters for BCSO are rather far from the model with an exact SU(4) symmetry [10]. Moreover, the spin-orbit coupling (SOC) and the directional dependence of the orbital hopping usually break both the spin-space and orbital-space SU(2) symmetries, as exemplified in iridates [11]. Thus, it would

seem even more difficult to realize an SU(N)-symmetric system in real magnets with SOC. (See Refs. [12–15] for proposed realization of SU(N) symmetry. However, they do not lead to QSOL because of their crystal structures.)

In this Letter, we demonstrate a novel mechanism for realizing an SU(4) spin system in a solid-state system with an onsite SOC. Paradoxically, the symmetry of the spin-orbital space can be *enhanced* to SU(4) when the SOC is strong. In particular, we propose α -ZrCl₃ [16–18] as the first candidate for an SU(4)-symmetric QSOL on the honeycomb lattice. Its d^1 electronic configuration in the octahedral ligand field, combined with the strong SOC, implies that the ground state of the electron is described by a $J_{\text{eff}} = 3/2$ quartet [19]. In fact, the resulting effective Hamiltonian appears to be anisotropic in the quartet space. Nevertheless, we show that the model is gauge-equivalent to an SU(4)-symmetric Hubbard model. In the strong repulsion limit, its low-energy effective Hamiltonian is the Kugel-Khomskii model [20] on the honeycomb lattice, exactly at the SU(4) symmetric point:

$$H_{\text{eff}} = J \sum_{\langle ij \rangle} \left(\mathbf{S}_i \cdot \mathbf{S}_j + \frac{1}{4} \right) \left(\mathbf{T}_i \cdot \mathbf{T}_j + \frac{1}{4} \right), \quad (1)$$

where $J > 0$, and \mathbf{S}_j and \mathbf{T}_j are pseudospin-1/2 operators defined for each site j . The SU(4) symmetry can be made manifest by rewriting the Hamiltonian, up to a constant shift, as $H_{\text{eff}} = \frac{J}{4} \sum_{\langle ij \rangle} P_{ij}$, where the spin state at each site forms the fundamental representation of SU(4), and P_{ij} is the operator which swaps the states at sites i and j . This is a natural generalization of the antiferromagnetic SU(2) Heisenberg model to SU(4).

The ground state of the SU(2) spin-1/2 antiferromagnet on the honeycomb lattice is simply Néel-ordered [21,

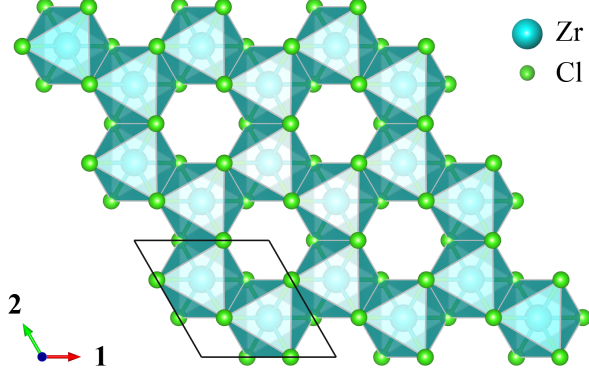


FIG. 1. Geometric structure of honeycomb α -ZrCl₃. Cyan and light green spheres represent Zr and Cl, respectively. The crystallographic axes are shown and labelled as the 1- and 2-directions.

22], reflecting the unfrustrated nature of the lattice. On the other hand, the $SU(N)$ generalization of the Néel state by putting different flavors on neighboring sites gives a macroscopic number of classical ground states when $N > 2$ [23–25], implying its instability. In fact, it was argued that the $SU(4)$ antiferromagnet on the honeycomb lattice has a QSOL ground state without any long-range order [5, 6].

Candidate materials. — As we mentioned in the Introduction, we propose α -ZrCl₃ with a honeycomb geometry as the first candidate for the d^1 honeycomb system, as shown in Fig. 1. More generally, we consider the class of materials α - MX_3 , with $M = \text{Ti, Zr, Hf, etc.}$, $X = \text{F, Cl, Br, etc.}$. Their crystal structure is almost the same as that of α -RuCl₃, which is known to be an approximate realization of the Kitaev honeycomb model [26, 27]. However, the electronic structure of α - MX_3 is different from α -RuCl₃: here, M is in the $3+$ state with a d^1 electronic configuration in the octahedral ligand field. Our strategy for the realization of $SU(4)$ spin models starts with a low-energy quartet of electronic states with the effective angular momentum $J_{\text{eff}} = 3/2$ on each M .

For this description to be valid, the SOC has to be strong enough. As the atomic number increases from Ti to Hf, SOC gets stronger and the description by the effective angular momentum becomes exact. The compounds α - $M\text{Cl}_3$ with $M = \text{Ti, Zr}$ and related Na_2VO_3 have been already reported experimentally. For α -TiCl₃, a structural transition and opening of the spin gap at $T = 217$ K have been reported [28]. This implies a small SOC, as it is consistent with a massively degenerate manifold of spin-singlets expected in the limit of a vanishing SOC [29]. In compounds with heavier elements, the strong SOC can convert this extensively degenerate manifold of product

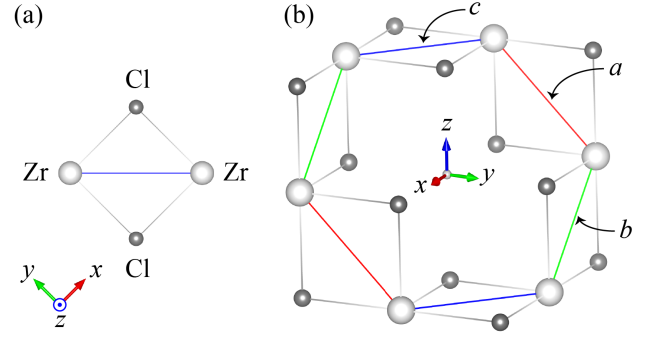


FIG. 2. (a) Superexchange pathways between two Zr ions connected by a c -bond (blue) in α -ZrCl₃. White and grey spheres represent Zr and Cl atoms, respectively. (b) Three different types of bonds in α -ZrCl₃. Red, light green, and blue bonds represent a -, b -, and c -bonds on the yz -, zx -, and xy -planes, respectively.

states into a resonating quantum state. Thus, we expect realization of the $SU(4)$ QSOL due to strong SOC with metal ions heavier than Ti. In the following, we pick up α -ZrCl₃ as an example, although the same analysis should apply to α -HfCl₃, and $A_2M'O_3$ ($A = \text{Na, Li, etc.}$, $M' = \text{Nb, Ta, etc.}$) as well.

Effective Hamiltonian. — In the strong ligand field, the description with one electron in the threefold degenerate t_{2g} -shell for α -ZrCl₃ becomes exact. We denote these d_{yz} , d_{zx} , and d_{xy} -orbitals by a , b , c , respectively. Let $a_{j\sigma}$, $b_{j\sigma}$ and $c_{j\sigma}$ represent annihilation operators on these orbitals on the j -th site of Zr^{3+} with spin- σ , and $n_{\xi\sigma j}$ with $\xi \in \{a, b, c\}$ be the corresponding number operators. We also use this $(a, b, c) = (yz, zx, xy)$ notation to label bonds: each Zr — Zr bond is called ξ -bond ($\xi = a, b, c$) when the superexchange pathway is on the ξ -plane [30], as illustrated in Fig. 2.

We define a $J_{\text{eff}} = 3/2$ quartet spinor as $\psi = (\psi_{\uparrow\uparrow}, \psi_{\uparrow\downarrow}, \psi_{\downarrow\uparrow}, \psi_{\downarrow\downarrow})^t = (\psi_{3/2}, \psi_{-3/2}, \psi_{1/2}, \psi_{-1/2})^t$, where ψ_{J^z} is the annihilation operator for the $|J = 3/2, J^z\rangle$ state. Assuming the SOC is the largest electronic energy scale, except for the ligand field splitting, fermionic operators can be rewritten by the quartet $\psi_{j\tau\sigma}$ as follows.

$$a_{j\sigma}^\dagger = \frac{\sigma}{\sqrt{6}}(\psi_{j\uparrow\bar{\sigma}}^\dagger - \sqrt{3}\psi_{j\downarrow\sigma}^\dagger), \quad (2)$$

$$b_{j\sigma}^\dagger = \frac{i}{\sqrt{6}}(\psi_{j\uparrow\bar{\sigma}}^\dagger + \sqrt{3}\psi_{j\downarrow\sigma}^\dagger), \quad (3)$$

$$c_{j\sigma}^\dagger = \sqrt{\frac{2}{3}}\psi_{j\uparrow\sigma}^\dagger, \quad (4)$$

where the indices τ and σ of $\psi_{j\tau\sigma}$ label the pseudoorbital and pseudospin indices, respectively. We begin from the

following Hubbard Hamiltonian for α -ZrCl₃,

$$H = -t \sum_{\sigma, \langle ij \rangle \in \alpha} (\beta_{i\sigma}^\dagger \gamma_{j\sigma} + \gamma_{i\sigma}^\dagger \beta_{j\sigma}) + h.c. + \frac{U}{2} \sum_{j, (\delta, \sigma) \neq (\delta', \sigma')} n_{\delta\sigma j} n_{\delta'\sigma' j}, \quad (5)$$

where t is a real-valued hopping parameter through the hopping shown in Fig. 2(a), $U > 0$ is the Hubbard interaction, $\langle ij \rangle \in \alpha$ means that the bond $\langle ij \rangle$ is an α -bond, $\langle \alpha, \beta, \gamma \rangle$ runs over every cyclic permutation of $\langle a, b, c \rangle$, and $\delta, \delta' \in \{a, b, c\}$. By inserting Eqs. (2)-(4), we get

$$H = -\frac{t}{\sqrt{3}} \sum_{\langle ij \rangle} \psi_i^\dagger U_{ij} \psi_j + h.c. + \frac{U}{2} \sum_j \psi_j^\dagger \psi_j (\psi_j^\dagger \psi_j - 1), \quad (6)$$

where ψ_j is the $J_{\text{eff}} = 3/2$ spinor on the j th site, and $U_{ij} = U_{ji}$ is a 4×4 matrix

$$U_{ij} = \begin{cases} U^a = \tau^y \otimes I_2 & (\langle ij \rangle \in a) \\ U^b = -\tau^x \otimes \sigma^z & (\langle ij \rangle \in b) \\ U^c = -\tau^x \otimes \sigma^y & (\langle ij \rangle \in c) \end{cases}, \quad (7)$$

where I_m is the $m \times m$ identity matrix, while τ and σ are Pauli matrices acting on the τ and σ indices of $\psi_{j\tau\sigma}$, respectively. We note that $U^{a,b,c}$ are unitary and Hermitian, and thus $U_{ji} = U_{ij}^\dagger = U_{ij}$.

Now we consider a (local) SU(4) gauge transformation,

$$\psi_j \rightarrow g_j \cdot \psi_j, \quad U_{ij} \rightarrow g_i U_{ij} g_j^\dagger, \quad (8)$$

where g_j is an element of SU(4) defined for each site j . For every loop C on the lattice, the SU(4) flux defined by the product $\prod_{\langle ij \rangle \in C} U_{ij}$ is invariant under the gauge transformation.

Remarkably, for each elementary hexagonal loop (which we call plaquette) p in the honeycomb lattice with the coloring illustrated in Fig. 2(b),

$$\prod_{\langle ij \rangle \in p} U_{ij} = U^a U^b U^c U^a U^b U^c = (U^a U^b U^c)^2 = -I_4, \quad (9)$$

which corresponds to just an Abelian phase π . Since all the flux operators on the honeycomb lattice can be made of some product of these plaquettes, there is an SU(4) gauge transformation to reduce the model (6) to the π -flux Hubbard model H with a global SU(4) symmetry, as proven in Sec. A of SM [31].

$$H = -\frac{t}{\sqrt{3}} \sum_{\langle ij \rangle} \eta_{ij} \psi_i^\dagger \psi_j + h.c. + \frac{U}{2} \sum_j \psi_j^\dagger \psi_j (\psi_j^\dagger \psi_j - 1), \quad (10)$$

where the definition of $\eta_{ij} = \pm 1$, arranged to insert a π flux inside each plaquette, is included in Sec. A of SM [31]. At quarter filling, i.e. one electron per site, which is the case in α -ZrCl₃, the system becomes a Mott

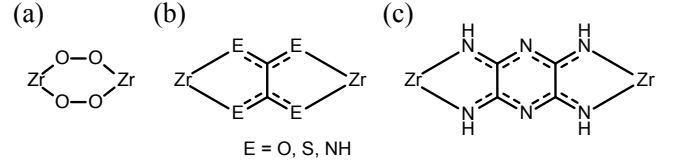


FIG. 3. Other possible superexchange pathways between two metal ions. (a) Zr — O — O — Zr. (b) Oxalate-based metal-organic motif. ($E = \text{O, S, NH}$) (c) Tetraaminopyrazine-bridged metal-organic motif.

insulator for a sufficiently large $U/|t|$. The low-energy effective Hamiltonian for the spin and orbital degrees of freedom, obtained by the second-order perturbation theory in t/U , is the Kugel-Khomskii model exactly at the SU(4) point (1), with $\mathbf{S} = \boldsymbol{\sigma}/2$, $\mathbf{T} = \boldsymbol{\tau}/2$, and $J = 8t^2/(3U)$ in the transformed basis set. We note that the effective Hamiltonian does not depend on the phase factor η_{ij} , as it cancels out in the second-order perturbation in t/U . Corboz *et al.* argued that this SU(4) Heisenberg model on the honeycomb lattice hosts a gapless QSOL [5]. Therefore, we have found a possible realization of gapless QSOL in α -ZrCl₃ with an *emergent* SU(4) symmetry.

The nontrivial nature of this model may be understood in terms of the Lieb-Schultz-Mattis-Affleck (LSMA) theorem for the SU(N) spin systems [25, 32–34], generalized to higher dimensions [32, 35–38]. As a result, under the SU(N) symmetry and the translation symmetry, the ground state of the SU(N) spin system with n spins of the fundamental representation per unit cell cannot be unique, if there is a non-vanishing excitation gap and n/N is not an integer. This rules out a featureless Mott insulator phase, which is defined as a gapped phase with a unique ground state, namely without any spontaneous symmetry breaking or topological order.

For the honeycomb lattice ($n = 2$) there is no LSMA constraint for an SU(2) spin system [39]. Nevertheless, for the SU(4) spin system we discuss in this Letter, a two-fold ground-state degeneracy is required to open the gap. This suggests the stability of a gapless QSOL phase of the SU(4) Heisenberg model on the honeycomb lattice. Especially, assuming the π -flux Dirac spin-orbital liquid ansatz proposed in Ref. [5] is correct, a mass gap for the Dirac spectrum is forbidden unless the SU(4) or translation symmetry is broken. Detailed analysis based on the LSMA theorem will be discussed in a separate publication [40].

Other possible structures. — In addition to three-dimensional (3D) inorganic polymorphs [31], metal-organic frameworks (MOFs) with motifs listed in Fig. 3 are an interesting playground to explore a variety of SU(4) QSOLs. It was recently argued [41] that Kitaev spin liquids can be realized in MOFs by a mechanism similar to the one in iridates [11]. Since the present deriva-

tion of an emergent SU(4) symmetry shares the same t_{2g} hopping model as in Ref. [11], it is also expected to apply to Zr- or Hf-based MOFs. While Fig. 3(a) is the longer superexchange pathways expected in oxides similar to triangular iridates [42], Fig. 3(b) and (c) show the superexchange pathways possible in Zr- or Hf-based MOFs. With these oxalate- or tetraaminopyrazine-based ligands, we can expect the two independent superexchange pathways similar to α -ZrCl₃ as discussed in Ref. [41].

Following the case of the honeycomb lattice, we can repeat the same analysis to derive the effective spin-orbital model for each 3D tricoordinated lattice. Recently, the classification of spin liquids on various tricoordinated lattices attracts much attention, so it is worth investigating [43–45]. All the tricoordinated lattices considered in this Letter are listed in Table I. The Table is based on the classification of tricoordinated nets by Wells [46]. We use a Schläfli symbol (p, c) to label a lattice, where p is the shortest elementary loop length of the lattice, and $c = 3$ means the tricoordination of the vertices. For example, (6,3) is the two-dimensional (2D) honeycomb lattice, and all the other lattices are 3D tricoordinated lattices, distinguished by additional letters following Wells [46]. $8^2.10-a$ is a nonuniform lattice and, thus, the notation is different from the other lattices.

Generalizing the discussion on the honeycomb lattice, if the SU(4) flux for any loop C is reduced to an Abelian phase ζ_C as $\prod_{\langle ij \rangle \in C} U_{ij} = \zeta_C I_4$ (for $\forall C$), the Hubbard model acquires the SU(4) symmetry. We have examined [31, 40] this for each lattice in Table I, where a checkmark is put on the SU(4) column if the above condition holds. Moreover, in order to form a stable structure with the present mechanism, the bonds from each site must form 120 degrees and an octahedral coordination. This condition is again checked for each lattice, and indicated in the 120° bond column [45] of Table I. We also put a checkmark on the LSMA column, when the LSMA theorem implies a ground state degeneracy or gapless excitations for the SU(4)-symmetric Hubbard model. For example, the LSMA constraint applies to the (8,3)- b lattice, since $n/N = 6/4$ is fractional.

Crystalline spin-orbital liquids. — Finally, we would like to discuss the generalization of the concept of crystalline spin liquids (XSL) [48] to SU(4)-symmetric systems. In the context of gapless Kitaev spin liquids as proposed in Ref. [48], a crystalline spin liquid is defined as a spin liquid state where a gapless point (or a gapped topological phase) is protected not just by the unbroken time-reversal or translation symmetry, but by the space group symmetry of the lattice. In the (10,3) lattices listed in Table I, the unit cell consists of a multiple of 4 sites, and thus the generalized LSMA theorem seems to allow a featureless insulator if we only consider the translation.

Following Refs. [49–51], however, we can effectively reduce the size of the unit cell by dividing the unit cell by the nonsymmorphic symmetry, and thus the filling

TABLE I. Tricoordinated lattices discussed in this Letter. Space groups are shown in number indices. Nonsymmorphic ones are underlined. n is the number of sites per unit cell.

Wells' notation	Lattice name	SU(4)	120° bond	n	Space group	LSMA
(10,3)- a	hyperoctagon	✓ ^a	✓	4	214	✓ ^b
(10,3)- b	hyperhoneycomb	✓ ^a	✓	4	70	✓ ^b
(10,3)- d	—	✓ ^a	—	8	52	✓ ^b
(9,3)- a	hypernonagon	—	—	12	166	—
$8^2.10-a$	—	✓	✓	8	141	—
(8,3)- b	hyperhexagon	✓	✓	6	166	✓ ^c
—	stripyhoneycomb	✓	✓	8	66	—
(6,3)	2D honeycomb	✓	✓	2		✓ ^d

^a The product of hopping matrices along every elementary loop is unity, resulting in the SU(4) Hubbard model with zero flux.

^b Nonsymmorphic symmetries of the lattice are enough to protect a QSOL state, i.e. hosting an XSOL state.

^c Although the model has a π flux, with an appropriate gauge choice the unit cell is not enlarged. Therefore, the LSMA theorem straightforwardly applies to the π -flux SU(4) Hubbard model.

^d While the standard LSMA theorem is not effective for the π -flux SU(4) Hubbard model here, the magnetic translation symmetry works to protect a QSOL state [47].

constraint becomes tighter with a nonsymmorphic space group. Even in the (10,3) lattices, the gapless QSOL state can be protected by the further extension of the LSMA theorem [40]. We call them crystalline spin-orbital liquids (XSOLs) in the sense that these exotic phases are protected in the presence of both the SU(4) symmetry and (nonsymmorphic) space group symmetries. We put a checkmark on the LSMA column of Table I if either the standard or extended LSMA theorem applies.

Discussions. — We found that, as a consequence of the combination of the octahedral ligand field and SOC, SU(4) symmetry *emerges* in α -ZrCl₃. In addition to the ZrCl₃ (or $A_2M'O_3$ [31]) family we have discussed, Zr- or Hf-based MOFs could also realize SU(4) Heisenberg models on various tricoordinated lattices. Especially, 3D (10,3)- a [52], (10,3)- b [53], and $8^2.10-a$ [48, 54] lattices, as well as the 2D honeycomb lattice [55], were already realized in some MOFs with an oxalate ligand. Thus we can expect that microscopic models defined by Eq. (5) on various tricoordinated lattices will apply in the same way as the honeycomb α -ZrCl₃ if we replace the metal ions of these MOFs with Zr³⁺, Hf³⁺, Nb⁴⁺, or Ta⁴⁺ [41].

It would be also interesting to investigate SU(4) Heisenberg models on nontricoordinated lattices. Especially, on the lattice with 1 or 3 sites per unit cell, the LSMA theorem can exclude the possibility of a simply gapped \mathbb{Z}_2 spin liquid and suggests a \mathbb{Z}_4 QSOL or new symmetry-enriched topological phases instead.

Experimentally, muon spin resonance or nuclear magnetic resonance (NMR) experiments can rule out the ex-

istence of long-range magnetic ordering or spin freezing in the spin sector. In the orbital sector, a possible experimental signature to observe the absence of orbital ordering or freezing should be finite-frequency electron spin resonance (ESR) [56] or extended X-ray absorption fine structure [9]. Especially, finite-frequency ESR can observe the dynamical Jahn-Teller (JT) effect [57, 58], where the g -factor isotropy directly signals the quantum fluctuation between different orbitals [56, 59, 60]. This is applicable to our case because of the shape difference in the $J_{\text{eff}} = 3/2$ orbitals [19], and the static JT distortion will result in the anisotropy in the in-plane g -factors [61] [62]. In addition, the specific heat or thermal transport measurements can distinguish between the gapped and gapless spectra. The emergent SU(4) symmetry would result in changing the universality class of critical phenomena, or in the accidental coincidence between the time scales of two different excitations for spins and orbitals observed by NMR and ESR, respectively.

Note added. — Following the early version of the present paper on arXiv, a microscopic derivation of the SU(4) model on the hyperhoneycomb lattice has been reported [63].

We thank A. Banisafar, K. Collins, K. Damle, E. Demler, V. Dwivedi, S. Ebihara, D. E. Freedman, Y. Fuji, B. I. Halperin, M. Hermanns, H. Katsura, G. Khaliullin, D. I. Khomskii, R. Kobayashi, M. Lajkó, L. Li, F. Mila, Y. Nakagawa, J. Romhányi, R. Sano, K. Shtengel, A. Smerald, T. Soejima, H. Takagi, T. Takayama, T. Senthil, S. Tsuneyuki, and, especially, I. Kimchi, for helpful comments. The crystal structure was taken from Materials Project. M.G.Y. is supported by the Materials Education program for the future leaders in Research, Industry, and Technology (MERIT), and by JSPS. This work was supported by JSPS KAKENHI Grant Numbers JP15H02113, JP17J05736, and JP18H03686, and by JSPS Strategic International Networks Program No. R2604 “TopoNet”. We also acknowledge the support of the Max-Planck-UBC-UTokyo Centre for Quantum Materials. M.G.Y. acknowledges the Quantum Materials Department at MPI-FKF, Stuttgart for kind hospitality during his visits.

* m.yamada@issp.u-tokyo.ac.jp

† Also at Andronikashvili Institute of Physics, 0177 Tbilisi, Georgia.

- [1] L. Balents, *Nature (London)* **464**, 199 (2010).
- [2] L. Savary and L. Balents, *Rep. Prog. Phys.* **80**, 016502 (2017).
- [3] Y. Q. Li, M. Ma, D. N. Shi, and F. C. Zhang, *Phys. Rev. Lett.* **81**, 3527 (1998).
- [4] M. Hermele and V. Gurarie, *Phys. Rev. B* **84**, 174441 (2011).
- [5] P. Corboz, M. Lajkó, A. M. Läuchli, K. Penc, and F. Mila, *Phys. Rev. X* **2**, 041013 (2012).
- [6] M. Lajkó and K. Penc, *Phys. Rev. B* **87**, 224428 (2013).
- [7] M. Cazalilla and A. Rey, *Rep. Prog. Phys.* **77**, 124401 (2014).
- [8] H. D. Zhou, E. S. Choi, G. Li, L. Balicas, C. R. Wiebe, Y. Qiu, J. R. D. Copley, and J. S. Gardner, *Phys. Rev. Lett.* **106**, 147204 (2011).
- [9] S. Nakatsuji, K. Kuga, K. Kimura, R. Satake, N. Katayama, E. Nishibori, H. Sawa, R. Ishii, M. Hagiwara, F. Bridges, T. U. Ito, W. Higemoto, Y. Karaki, M. Halim, A. A. Nugroho, J. A. Rodriguez-Rivera, M. A. Green, and C. Broholm, *Science* **336**, 559 (2012).
- [10] A. Smerald and F. Mila, *Phys. Rev. B* **90**, 094422 (2014).
- [11] G. Jackeli and G. Khaliullin, *Phys. Rev. Lett.* **102**, 017205 (2009).
- [12] F. J. Ohkawa, *J. Phys. Soc. Jpn.* **52**, 3897 (1983).
- [13] R. Shiina, H. Shiba, and P. Thalmeier, *J. Phys. Soc. Jpn.* **66**, 1741 (1997).
- [14] F. Wang and A. Vishwanath, *Phys. Rev. B* **80**, 064413 (2009).
- [15] K. I. Kugel, D. I. Khomskii, A. O. Sboychakov, and S. V. Streltsov, *Phys. Rev. B* **91**, 155125 (2015).
- [16] B. Swaroop and S. N. Flengas, *Can. J. Chem.* **42**, 1495 (1964).
- [17] B. Swaroop and S. N. Flengas, *Can. J. Phys.* **42**, 1886 (1964).
- [18] G. Brauer, *Handbuch der Präparativen Anorganischen Chemie, Bd. II* (Ferdinand Enke Verlag, Stuttgart, 1978).
- [19] J. Romhányi, L. Balents, and G. Jackeli, *Phys. Rev. Lett.* **118**, 217202 (2017).
- [20] K. I. Kugel and D. I. Khomskii, *Sov. Phys. Usp.* **25**, 231 (1982).
- [21] J. D. Reger, J. A. Riera, and A. P. Young, *J. Phys. Condens. Matter.* **1**, 1855 (1989).
- [22] J. Fouet, P. Sindzingre, and C. Lhuillier, *Eur. Phys. J. B* **20**, 241 (2001).
- [23] M. Hermele, V. Gurarie, and A. M. Rey, *Phys. Rev. Lett.* **103**, 135301 (2009).
- [24] A. V. Gorshkov, M. Hermele, V. Gurarie, C. Xu, P. S. Julianne, J. Ye, P. Zoller, E. Demler, M. D. Lukin, and A. M. Rey, *Nat. Phys.* **6**, 289 (2010).
- [25] M. Lajkó, K. Wamer, F. Mila, and I. Affleck, *Nucl. Phys. B* **924**, 508 (2017).
- [26] A. Kitaev, *Ann. Phys.* **321**, 2 (2006), january Special Issue.
- [27] K. W. Plumb, J. P. Clancy, L. J. Sandilands, V. V. Shankar, Y. F. Hu, K. S. Burch, H.-Y. Kee, and Y.-J. Kim, *Phys. Rev. B* **90**, 041112 (2014).
- [28] S. Ogawa, *J. Phys. Soc. Jpn.* **15**, 1901 (1960).
- [29] G. Jackeli and D. A. Ivanov, *Phys. Rev. B* **76**, 132407 (2007).
- [30] The Cartesian xyz axes are defined as in Fig. 2(b).
- [31] See Supplemental Material at [URL will be inserted by publisher] for more details.
- [32] E. Lieb, T. Schultz, and D. Mattis, *Ann. Phys.* **16**, 407 (1961).
- [33] I. Affleck and E. H. Lieb, *Lett. Math. Phys.* **12**, 57 (1986).
- [34] Y. Yao, C.-T. Hsieh, and M. Oshikawa, arXiv:1805.06885 [cond-mat.str-el].
- [35] I. Affleck, *Phys. Rev. B* **37**, 5186 (1988).
- [36] M. Oshikawa, *Phys. Rev. Lett.* **84**, 1535 (2000).
- [37] M. B. Hastings, *Europhys. Lett.* **70**, 824 (2005).
- [38] K. Totsuka, “Lieb-Schultz-Mattis approach to SU(N)-

- symmetric Mott insulators,” JPS 72nd Annual Meeting (2017).
- [39] C.-M. Jian and M. Zaletel, Phys. Rev. B **93**, 035114 (2016).
 - [40] M. G. Yamada, M. Oshikawa, and G. Jackeli, To be published.
 - [41] M. G. Yamada, H. Fujita, and M. Oshikawa, Phys. Rev. Lett. **119**, 057202 (2017).
 - [42] A. Catuneanu, J. G. Rau, H.-S. Kim, and H.-Y. Kee, Phys. Rev. B **92**, 165108 (2015).
 - [43] M. Hermanns, K. O’Brien, and S. Trebst, Phys. Rev. Lett. **114**, 157202 (2015).
 - [44] M. Hermanns, S. Trebst, and A. Rosch, Phys. Rev. Lett. **115**, 177205 (2015).
 - [45] K. O’Brien, M. Hermanns, and S. Trebst, Phys. Rev. B **93**, 085101 (2016).
 - [46] A. F. Wells, *Three-dimensional Nets and Polyhedra* (Wiley, New York, 1977).
 - [47] Y.-M. Lu, Y. Ran, and M. Oshikawa, arXiv:1705.09298 [cond-mat.str-el].
 - [48] M. G. Yamada, V. Dwivedi, and M. Hermanns, Phys. Rev. B **96**, 155107 (2017).
 - [49] S. A. Parameswaran, A. M. Turner, D. P. Arovas, and A. Vishwanath, Nat. Phys. **9**, 299 (2013).
 - [50] H. Watanabe, H. C. Po, A. Vishwanath, and M. Zaletel, Proc. Natl. Acad. Sci. USA **112**, 14551 (2015).
 - [51] H. C. Po, H. Watanabe, C.-M. Jian, and M. P. Zaletel, Phys. Rev. Lett. **119**, 127202 (2017).
 - [52] E. Coronado, J. R. Galán-Mascarós, C. J. Gómez-García, and J. M. Martínez-Agudo, Inorg. Chem. **40**, 113 (2001).
 - [53] B. Zhang, Y. Zhang, and D. Zhu, Dalton Trans. **41**, 8509 (2012).
 - [54] M. Clemente-León, E. Coronado, and M. López-Jordà, Dalton Trans. **42**, 5100 (2013).
 - [55] B. Zhang, Y. Zhang, Z. Wang, D. Wang, P. J. Baker, F. L. Pratt, and D. Zhu, Sci. Rep. **4**, 6451 (2014).
 - [56] Y. Han, M. Hagiwara, T. Nakano, Y. Nozue, K. Kimura, M. Halim, and S. Nakatsuji, Phys. Rev. B **92**, 180410 (2015).
 - [57] J. Nasu and S. Ishihara, Phys. Rev. B **88**, 094408 (2013).
 - [58] J. Nasu and S. Ishihara, Phys. Rev. B **91**, 045117 (2015).
 - [59] I. Bersuker, Coord. Chem. Rev. **14**, 357 (1975).
 - [60] A. Abragam and B. Bleaney, *Electron Paramagnetic Resonance of Transition Ions* (Clarendon Press, Oxford, 1970).
 - [61] N. Iwahara, V. Vieru, L. Ungur, and L. F. Chibotaru, Phys. Rev. B **96**, 064416 (2017).
 - [62] We note that the trigonal distortion existing *a priori* in real materials only splits the degeneracy between the out-of-plane and in-plane *g*-factors, and the splitting of the two in-plane modes clearly indicates an additional (e.g. tetragonal) distortion.
 - [63] W. M. H. Natori, E. C. Andrade, and R. G. Pereira, arXiv:1802.00044 [cond-mat.str-el].

Supplemental Material for “Emergent SU(4) Symmetry in α -ZrCl₃ and Crystalline Spin-Orbital Liquids”

Masahiko G. Yamada,¹ Masaki Oshikawa,¹ and George Jackeli^{2,3,*}

¹*Institute for Solid State Physics, University of Tokyo, Kashiwa 277-8581, Japan.*

²*Institute for Functional Matter and Quantum Technologies,*

University of Stuttgart, Pfaffenwaldring 57, D-70569 Stuttgart, Germany.

³*Max Planck Institute for Solid State Research, Heisenbergstrasse 1, D-70569 Stuttgart, Germany.*

In this Supplemental Material, we have Section A: Boundary condition effects on the SU(N) gauge transformation, Section B: Hidden SO(4) symmetry in the Hund coupling, and Section C: Flux sectors for various tricoordinated lattices.

Section A: Boundary condition effects on the SU(N) gauge transformation

First, we begin from the one-dimensional (1D) Hubbard model with an open boundary condition (OBC).

$$H_{1\text{DOBC}} = -t \sum_{j=1}^{L-1} \psi_j^\dagger U_{j,j+1} \psi_{j+1} + h.c. + \frac{U}{2} \sum_{j=1}^L \psi_j^\dagger \psi_j (\psi_j^\dagger \psi_j - 1), \quad (1)$$

where L is a system size, ψ_j is a N -component spinor, $U_{j,j+1}$ is an $N \times N$ unitary matrix defined on the j th site, and t and U are real-valued hopping and Hubbard terms, respectively. The (local) gauge transformation is simply given by the following string operator g_j .

$$g_j = \prod_{k=1}^{j-1} U_{k,k+1}, \quad (2)$$

$$\psi'_j = g_j \cdot \psi_j, \quad (3)$$

$$U'_{j,j+1} = g_j U_{j,j+1} g_{j+1}^\dagger = I_N, \quad (4)$$

where I_m is the $m \times m$ identity matrix. Thus, 1D Hubbard model with OBC is a trivial case where we can always make it SU(N)-symmetric.

$$H_{1\text{DOBC}} = -t \sum_{j=1}^{L-1} \psi_j'^\dagger \psi'_{j+1} + h.c. + \frac{U}{2} \sum_{j=1}^L \psi_j'^\dagger \psi'_j (\psi_j'^\dagger \psi'_j - 1), \quad (5)$$

Therefore, in 1D electronic systems on a linear chain with nearest-neighbor hoppings only, if the $N \times N$ hopping matrices are all unitary, the tight-binding Hubbard model is trivially gauge-equivalent to the 1D SU(N) Hubbard model [1–4]. Such emergence of the SU(N) symmetry by the gauge transformation becomes more nontrivial in higher dimensions because there is a topological obstruction coming from the lattice geometry and also a possibility to realize topological ground state degeneracy, which is impossible in 1D systems [5].

Before going to higher dimensions, it is instructive to consider the 1D Hubbard model with a periodic boundary condition (PBC).

$$H_{1\text{DPBC}} = -t \sum_{j=1}^L \psi_j^\dagger U_{j,j+1} \psi_{j+1} + h.c. + \frac{U}{2} \sum_{j=1}^L \psi_j^\dagger \psi_j (\psi_j^\dagger \psi_j - 1), \quad (6)$$

where ψ_{L+1} is identified as ψ_1 . Clearly the gauge transformation does not change the flux inside the loop, so there is a necessary condition to have a gauge transformation which makes the Hamiltonian SU(N)-symmetric,

$$\prod_{j=1}^L U_{j,j+1} = \zeta I_N, \quad (7)$$

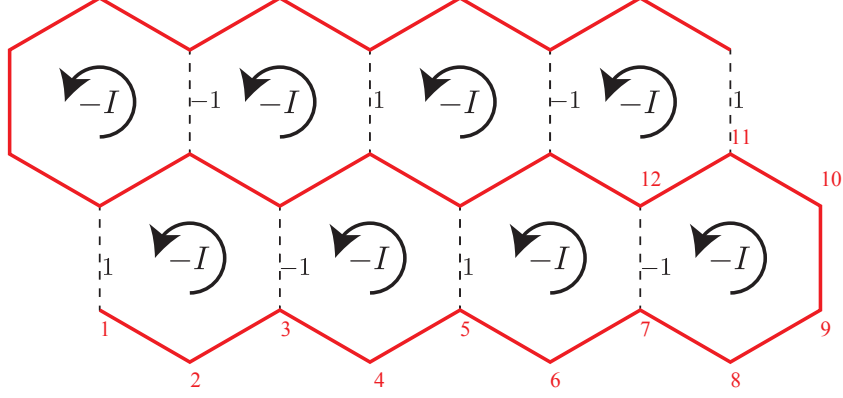


FIG. S1. Flake of the honeycomb lattice to show how the gauge transformation works for OBC. Along the red solid line, we used 1D gauge transformation and the flux constraints automatically determines the transformed hopping matrices for the rest of the bonds shown in black dashed lines.

with some $|\zeta| = 1$. This is also a sufficient condition. If we apply the same gauge transformation $g_j = \prod_{k=1}^{j-1} U_{k,k+1}$ as the OBC case for $j = 1, \dots, L$, the transformed matrices become

$$U'_{j,j+1} = \begin{cases} \prod_{k=1}^L U_{k,k+1} = \zeta I_N & (j = L) \\ I_N & (\text{otherwise}) \end{cases}. \quad (8)$$

Thus, the resulting Hamiltonian is completely $SU(N)$ -symmetric with a factor ζ ,

$$H_{1\text{DPBC}} = -t \left(\sum_{j=1}^{L-1} \psi_j^\dagger \psi'_{j+1} + \zeta \psi_L^\dagger \psi'_1 \right) + h.c. + \frac{U}{2} \sum_{j=1}^L \psi_j^\dagger \psi_j (\psi_j^\dagger \psi'_j - 1). \quad (9)$$

It must be noted that ζ cannot be eliminated by any gauge transformation and thus it is physical and called (magnetic) flux.

As for OBC, it is almost trivial to expand the proof of the existence of the gauge transformation to higher dimensions. This can be achieved by drawing the lattice with a single stroke of the brush. For simplicity, we use the finite-size two-dimensional (2D) honeycomb lattice with OBC. We begin from the following Hamiltonian.

$$H_{2\text{D}} = -\frac{t}{\sqrt{3}} \sum_{\langle ij \rangle} \psi_i^\dagger U_{ij} \psi_j + h.c. + \frac{U}{2} \sum_j \psi_j^\dagger \psi_j (\psi_j^\dagger \psi_j - 1), \quad (10)$$

where U_{ij} is again an $N \times N$ unitary matrix defined for each bond, and ψ_j is the N -component spinor on the j th site. Assuming each site is numbered in order for some nearest-neighbor site to have the subsequent number, we can do the same gauge transformation as the 1D OBC case. Again, this gauge transformation does not change the flux value for any loops, so there is a necessary condition to get a $SU(N)$ -symmetric model for each hexagonal plaquette (elementary loop) p .

$$\prod_{\langle ij \rangle \in p} U_{ij} = \zeta_p I_N \quad (\text{for } \forall p). \quad (11)$$

This condition is actually sufficient for OBC (assuming the existence of a single stroke path). We take a flake of the honeycomb lattice shown in Fig. S1. For simplicity, we use $\zeta_p = -1$ for $\alpha\text{-ZrCl}_3$ as discussed in the main text, but ζ_p can generally depend on each plaquette p .

If we draw a single stroke path shown as the red solid line in Fig. S1, all the unitary matrices on the red bonds become identity by the gauge transformation for the 1D red line. Remaining are black dashed bonds, but their hopping matrices are fixed by the flux condition (Eq. (11)). In the case of Fig. S1, around the bottom plaquettes the hopping matrices are determined from right to left because five of the surrounding matrices are made identity one by

one for each plaquette. By continuing this, all the unitary matrices are transformed into some η_{ij} times identity with $|\eta_{ij}| = 1$, and thus the Hamiltonian becomes completely $SU(N)$ -symmetric. We call this transformed gauge theorists' gauge.

$$H_{2D} = -\frac{t}{\sqrt{3}} \sum_{\langle ij \rangle} \eta_{ij} \psi_i^\dagger \psi_j' + h.c. + \frac{U}{2} \sum_j \psi_j^\dagger \psi_j' (\psi_j'^\dagger \psi_j' - 1), \quad (12)$$

where $\eta_{ij} = 1$ for red bonds, while the sign of $\eta_{ij} = \pm 1$ depends on each bond for black dashed bonds as indicated in Fig. S1 by the number near the black dashed bond. This is nothing but the model called a π -flux Hubbard model on the honeycomb lattice and the model can be constructed by changing the sign of the c -bonds alternately along the perpendicular direction. This gauge transformation effectively doubles the size of the unit cell.

Finally, we would like to discuss the 2D PBC case. In this case, we cannot find a gauge transformation, even if we assume the flux condition (Eq. (11)) for every hexagonal plaquette. The final obstructions to be considered are global (or topological) ones, which are two types of noncontractible loops on the 2D torus. The noncontractible loops in the same homotopy class are related by the flux conditions, so it is enough to consider only two noncontractible loops C_1 and C_2 along the 1- and 2-directions, respectively. Assuming the size of the torus to be $L_1 \times L_2$ original unit cells, the lengths of C_1 and C_2 become multiples of L_1 and L_2 , respectively. The necessary and sufficient conditions to find a gauge transformation in addition to Eq. (11) are two new flux conditions for C_1 and C_2 ,

$$\prod_{\langle ij \rangle \in C_1} U_{ij} = \zeta_{C_1} I_N, \quad \prod_{\langle ij \rangle \in C_2} U_{ij} = \zeta_{C_2} I_N. \quad (13)$$

In general these fluxes cannot be Abelian for any sets of unitary matrices U_{ij} . Thus, we specifically consider the model of α -ZrCl₃ discussed in the main text. In this model, all the hopping matrices are accidentally written by Pauli matrices, and their products only take some Pauli matrices times a complex number, which actually only takes 1, i , -1 , $-i$. In other words, their products are included in the Pauli group on 2 qubits. In this group, any element to the power of 4 becomes identity, so the flux inside the two noncontractible loops become trivial if both L_1 and L_2 are multiples of 4. This is a condition to find a gauge transformation to make the model explicitly $SU(N)$ -symmetric with a symmetric boundary condition, i.e. a boundary condition where both C_1 and C_2 have a zero flux. If we allow a more general boundary condition with a π flux inside C_1 or C_2 , then the conditions for L_1 or L_2 become milder.

Our effective model for the honeycomb α -ZrCl₃ was derived based on the superexchange interactions between the Zr³⁺ ions constructed from its geometry. However, similar superexchange interactions can also arise in the other structures listed in Fig. 3 in the main text, or in face-shared systems. We note that ZrCl₃ has some polymorphs and a chain compound β -ZrCl₃ with face-shared Cl octahedra [6] can also host a 1D $SU(4)$ Heisenberg model [4].

Since a nonlayered structure of Na₂VO₃ has already been reported [7], we can expect various three-dimensional (3D) polymorphs of ZrCl₃ or $A_2M'O_3$ with $A = \text{Na, Li}$ and $M' = \text{Nb, Ta}$, similarly to 3D β -Li₂IrO₃ [8] and γ -Li₂IrO₃ [9].

The generalization from the 2D case to the three-dimensional (3D) case is straightforward. The difference is that in 3 dimensions not all the fluxes of the plaquettes (or elementary loops in Section C) can be determined independently. This is called volume constraint and will be discussed in Section C.

Section B: Hidden $SO(4)$ symmetry in the Hund coupling

It is clear that the first apparent perturbation of an order $J_H/U \sim \mathcal{O}(0.1)$ is an onsite Hund coupling J_H . There are other possible perturbations like further-neighbor interactions, but we can expect that such effects are smaller than that of the Hund coupling similarly to α -RuCl₃. Actually, in the Kitaev materials like α -RuCl₃ the nearest-neighbor Kitaev interaction and the third-neighbor Heisenberg interaction are expected to be comparable [10], but this is probably due to fine tuning happening in the $J_{\text{eff}} = 1/2$ manifold and the Kitaev interaction has to be smaller than the naïve superexchange interaction expected in the whole t_{2g} orbitals because of the destructive interference which cancels out the direct hopping between the $J_{\text{eff}} = 1/2$ manifold [11]. In our $J_{\text{eff}} = 3/2$ models realized e.g. in α -ZrCl₃, such an accidental reduction of the highest-order contribution does not occur even in the nearest-neighbor interactions, so we expect the magnetic interaction in α -ZrCl₃ is much larger than the dominant Kitaev interaction in α -RuCl₃, and thus one- or two-order larger than the third-neighbor Heisenberg interactions in the case of α -ZrCl₃.

Next, in order to evaluate the effect of the Hund coupling, we will change the ordering of the $J_{\text{eff}} = 3/2$ bases to compare the model with a so-called $SO(5)$ -symmetric Hubbard model discussed in the literature on $S = 3/2$ cold atomic systems [12–14],

$$\psi = (\psi_{3/2}, \psi_{1/2}, \psi_{-1/2}, \psi_{-3/2})^t = (\psi_{\uparrow\uparrow}, \psi_{\downarrow\uparrow}, \psi_{\downarrow\downarrow}, \psi_{\uparrow\downarrow})^t. \quad (14)$$

In this basis it is easy to see a hidden $\text{SO}(4)$ symmetry, which is a subgroup of $\text{SO}(5) \simeq \text{Sp}(4) \subset \text{SU}(4)$ in the original model.

We will now show the Hund coupling in $\alpha\text{-ZrCl}_3$ actually possesses the $\text{SO}(5) \simeq \text{Sp}(4)$ symmetry, although the hopping matrices break a part of this symmetry. If we add a Hund coupling for the hopping model inside the t_{2g} orbitals [15], the Hamiltonian becomes

$$H = -t \sum_{\sigma, \langle ij \rangle \in \alpha} (\beta_{i\sigma}^\dagger \gamma_{j\sigma} + \gamma_{i\sigma}^\dagger \beta_{j\sigma}) + h.c. + \sum_j \left[\frac{U - 3J_H}{2} N_j(N_j - 1) - 2J_H \mathbf{s}_j^2 - \frac{J_H}{2} \mathbf{L}_j^2 + \frac{5}{2} J_H N_j \right], \quad (15)$$

where $\langle ij \rangle \in \alpha$ means that the bond $\langle ij \rangle$ is an α -bond, $\langle \alpha, \beta, \gamma \rangle$ runs over every cyclic permutation of $\langle a, b, c \rangle$, N_j is a number operator, \mathbf{s}_j is a total spin, and \mathbf{L}_j is a total effective angular momentum. Assuming a strong spin-orbit coupling limit $\lambda \gg |t|, J_H$, we project the Hilbert space onto the $J_{\text{eff}} = 3/2$ manifold. We note that we will ignore doublon/holon excitations with higher energies in the following discussions. In the original gauge before the gauge transformation, which we call lab gauge, the projected Hamiltonian becomes

$$H = -\frac{t}{\sqrt{3}} \sum_{\langle ij \rangle} \psi_i^\dagger V_{ij} \psi_j + h.c. + \sum_j \left[\frac{U - 3J_H}{2} \psi_j^\dagger \psi_j (\psi_j^\dagger \psi_j - 1) - \frac{4}{9} J_H \mathbf{J}_j^2 + \frac{5}{2} J_H \psi_j^\dagger \psi_j \right], \quad (16)$$

where $\mathbf{J}_j = \mathbf{s}_j + \mathbf{L}_j$ is a total effective angular momentum operator with a condition $J = 3/2$ after the projection, and

$$V_{ij} = \begin{cases} V^a = \tau^z \otimes \sigma^y = \Gamma^3 & (\langle ij \rangle \in a) \\ V^b = -\tau^z \otimes \sigma^x = -\Gamma^2 & (\langle ij \rangle \in b) \\ V^c = -\tau^y \otimes I_2 = \Gamma^1 & (\langle ij \rangle \in c) \end{cases}. \quad (17)$$

We used $\mathbf{s}_j = \mathbf{J}_j/3$ and $\mathbf{L}_j = 2\mathbf{J}_j/3$ inside the $J_{\text{eff}} = 3/2$ manifold derived from the Wigner-Eckart theorem. Thus, ignoring the hopping terms, the Hubbard and Hund couplings possess a hidden $\text{SO}(5) \simeq \text{Sp}(4)$ symmetry in the same way as the $S = 3/2$ cold atomic systems with a spin-preserving interaction.

The hopping term partially breaks this $\text{SO}(5)$ symmetry. To see this we use anticommuting Dirac gamma matrices in Ref. [12] defined as

$$(\Gamma^1, \Gamma^2, \Gamma^3, \Gamma^4, \Gamma^5) = (-\tau^y \otimes I_2, \tau^z \otimes \sigma^x, \tau^z \otimes \sigma^y, \tau^z \otimes \sigma^z, -\tau^x \otimes I_2). \quad (18)$$

Gamma matrices Γ^p ($p = 1, \dots, 5$) are forming an $\text{SO}(5)$ vector, which transforms as a vector in the same rotation for the hidden $\text{SO}(5)$ symmetry of the Hund coupling. There is no way to eliminate the non-Abelian hopping just by the $\text{SO}(5) \simeq \text{Sp}(4)$ gauge transformation, but we can rotate $\text{SO}(5)$ vectors locally to eliminate the bond dependence of the hopping.

For example, we can rotate all V_{ij} s to Γ^5 and then the Hamiltonian becomes almost uniform up to the same factors $\eta_{ij} = \pm 1$ as discussed in the previous section:

$$H = -\frac{t}{\sqrt{3}} \sum_{\langle ij \rangle} \eta_{ij} \psi_i^\dagger \Gamma^5 \psi_j' + h.c. + \sum_j \left[\frac{U - 3J_H}{2} \psi_j^\dagger \psi_j' (\psi_j'^\dagger \psi_j' - 1) - \frac{4}{9} J_H \mathbf{J}_j'^2 + \frac{5}{2} J_H \psi_j^\dagger \psi_j' \right]. \quad (19)$$

This model explicitly has a hidden $\text{SO}(4)$ symmetry because Γ^5 is invariant under the $\text{SO}(4)$ subgroup of the $\text{SO}(5)$ rotation which keeps a vector $(0, 0, 0, 0, 1)$ invariant. The last term is constant in the large $(U - 3J_H)$ limit at quarter filling, so the first meaningful contribution of an order $J_H/U \sim \mathcal{O}(0.1)$ would be the $\text{SO}(4)$ -invariant perturbation coming from the term $(4J_H/9) \mathbf{J}_j'^2$, which separates the degeneracy of the virtual state with two electrons per site into $J = 0$ and $J = 2$. However, this effect is again $\mathcal{O}(0.1)$ and, thus, we can expect this $\text{SU}(4)$ breaking perturbation to be negligible.

We note that the $\text{SO}(5) \simeq \text{Sp}(4)$ gauge transformation is just a subgroup of the $\text{SU}(4)$ gauge transformation, and it is not enough to go to “theorists’ gauge” without any non-Abelian hopping matrices. In fact, Dirac gamma matrices are not included in the generator of the $\text{Sp}(4)$ rotation for ψ and the rotation is generated by $\Gamma^{pq} = -(i/2)[\Gamma^p, \Gamma^q] = -i\Gamma^p \Gamma^q$ ($1 \leq p, q \leq 5$) [12]. Since the number of gamma matrices is conserved mod 2 by the $\text{SO}(5) \simeq \text{Sp}(4)$

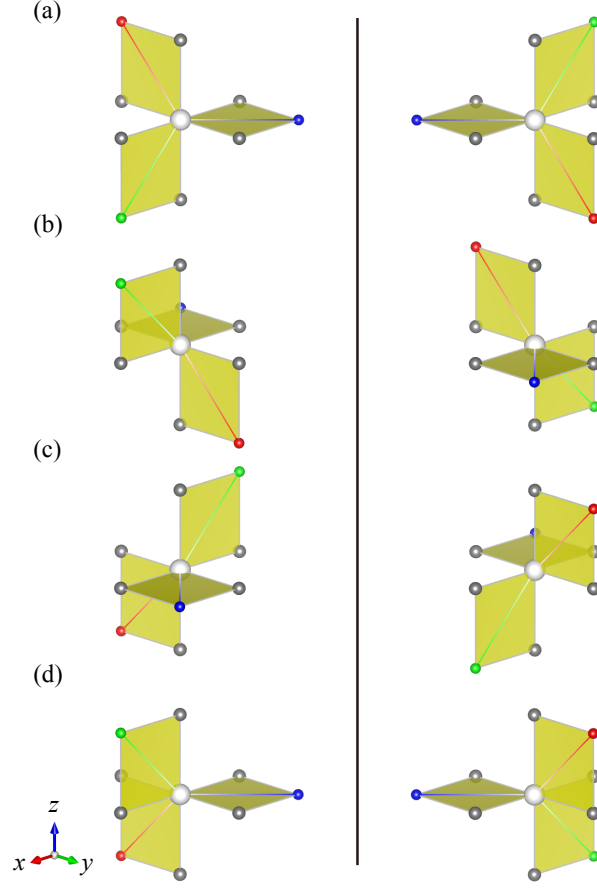


FIG. S2. All possible ways to connect three bonds in the 3D tricoordinated lattices. (a) is the same one as that in the 2D honeycomb lattice, while (b), (c), and (d) are produced by rotating (a) by 180° around the x , y , and z -axes. The left-hand side and the right-hand side are related by the inversion for each figure.

rotation, the hopping matrices written by one gamma matrix cannot be rotated to $SO(5)$ scalar by the $SO(5)$ gauge transformation, and this is why Γ^5 cannot be eliminated in Eq. (19).

In this analysis, we only considered the extreme limit $\lambda \gg J_H$ for simplicity to prove that the $SU(4)$ -breaking term comes from the order of $\mathcal{O}(0.1)$ by employing the $SO(5)$ gauge transformation intensively. While we no longer expect the existence of a hidden $SO(4)$ symmetry in a general case, it is not difficult to show that in the second-order perturbation the contribution breaking the original $SU(4)$ symmetry always involves a virtual state with an energy higher than the lowest order by λ or J_H . Anyway, we can conclude that, as long as we ignore higher order contributions of $\mathcal{O}(0.1)$, the emergent $SU(4)$ symmetry would be robust.

Section C: Flux sectors for various tricoordinated lattices

The flux sectors for the tricoordinated lattices listed in the main text can be treated similarly to the Kitaev models on tricoordinated lattices [16, 17] except for the difference in the gauge group. Following Kitaev [16], we use terminology of the lattice gauge theory. The link variables U_{ij} are Hermitian and unitary (in this case) 4×4 matrices defined for each bond (link) $\langle ij \rangle$ of the lattice. Each link variable depends on its type (color) of the bond as

$$U_{ij} = \begin{cases} U^a = \tau^y \otimes I_2 & (\langle ij \rangle \in a) \\ U^b = -\tau^x \otimes \sigma^z & (\langle ij \rangle \in b) , \\ U^c = -\tau^x \otimes \sigma^y & (\langle ij \rangle \in c) \end{cases} \quad (20)$$

TABLE S1. Flux sector of tricoordinated lattices. Only the flux value for the shortest elementary loops is shown here. Nonsymmorphic space group numbers are underlined. NS means that nonsymmorphic symmetries of the lattice are enough to protect a quantum spin-orbital liquid state. In addition to the contents of Table I in the main text, we also include O’Keeffe’s three-letter codes [18, 19].

Wells’ notation	Lattice name	O’Keeffe’s code	Minimal loop length	Flux sector	120-degree bond	Number of sites	Space group symbol	No.	LSMA constraints
(10,3)- <i>a</i>	hyperoctagon	srs	10	0-flux	✓	4	<i>I</i> ₄ 32	<u>214</u>	NS ✓
(10,3)- <i>b</i>	hyperhoneycomb	ths	10	0-flux	✓	4	<i>Fddd</i> ^a	<u>70</u>	NS ✓
(10,3)- <i>d</i>		utp	10	0-flux	—	8	<i>Pnna</i> ^b	<u>52</u>	NS ✓
nonuniform	8 ² .10- <i>a</i>	lig	8	π -flux	✓	8	<i>I</i> ₄ 1/ <i>amd</i>	<u>141</u>	—
(8,3)- <i>b</i>	hyperhexagon	etb	8	π -flux	✓	6	<i>R</i> $\bar{3}m$	166	✓
nonuniform	stripyhoneycomb	clh	6	π -flux	✓	8	<i>Cccm</i> ^c	<u>66</u>	—
(6,3)	2D honeycomb	hcb	6	π -flux	✓	2			✓

^a The most symmetric case should be *I*₄1/*amd*, including *Fddd*. Actually, *Fddd* is enough for the filling constraint.

^b There exists another phase with a *Pbcn* symmetry. Both symmetries are enough for the filling constraint.

^c There exists a more symmetric phase with a *P4₂/mmc* symmetry, but it is not enough for the filling constraint.

where τ and σ are independent Pauli matrices, following the original gauge (basis) used in the main text (not the one used in the previous section). The bond type *abc* is determined from which plane this bond belongs to, as discussed in the main text. We note that in the 3D case we actually have six types of bonds with additional ± 1 factors, so $U_{ij} = \pm U^a, \pm U^b, \pm U^c$ depending on a detailed structure of the bond $\langle ij \rangle$. This comes from the spatial dependence of the sign of the wavefunctions of the *d*-orbitals.

These additional ± 1 factors can simply be gauged out in the following way. In the 2D honeycomb lattice, there is no sign difference in the same bond type because all of them are related by the translation symmetry. In some 3D lattices, even if the two bonds belong to the same type, the hopping matrices can differ because they are related not by the translation symmetry, but by the screw or glide symmetry. Accompanied by the reflection or rotation, this symmetry can actually change the sign of the hopping matrix by -1 according to the shape of the t_{2g} -orbitals. When seen from the metal site, it is a 180° rotation around the *x*, *y*, or *z*-axis. If we consider the signs of the t_{2g} -orbitals, it is clear that 180° rotation changes the signs of some orbitals, while the inversion does not change the signs of the *d*-orbitals. As shown in Fig. S2, there are 8 types of metal sites, and all of them are related by some 180° rotation, which causes the sign difference, up to inversion. Fortunately, however, this additional sign can be eliminated by some gauge transformation, i.e. local rotations of the definition of the effective angular momentum $l = 1$ of the t_{2g} -orbitals. For example, if the metal site is rotated around the *x*-axis by 180° , the configuration of the surrounding ligands changes from Fig. S2(a) to Fig. S2(b). Then, according to the rotation, we rotate the definition of the angular momentum $l = 1$ around the *x*-axis by 180° , which can be done just by flipping the sign of the *yz*-orbital. Similarly, for the ones shown in Fig. S2(c), we just flip the sign of *zx*-orbital. Then, if we connect these two, Fig. S2(b) and (c), along the *xy*-plane, we obtain an additional -1 phase from this gauge transformation, and it completely cancels out the sign in question. If we do a similar local rotation in the fictitious orbital space for each metal site according to the physical 180° rotation, all the hopping matrices will be returned to the original ones in Eq. (20), and after all we do not have to care about the subtle difference among the same bond type. Thus, Eq. (20) is still valid after this “ \mathbb{Z}_2 ” gauge transformation.

In order to find a gauge transformation to get an SU(4) Hubbard model, we have to check that every Wilson loop operator is Abelian. In an abuse of language, each Wilson loop will be called flux inside the loop. We regard a Wilson loop operator I_4 as a zero flux, and $-I_4$ as a π flux. In order to get a desired gauge transformation, it is enough to show the flux inside every elementary loop *C* is Abelian:

$$\prod_{\langle ij \rangle \in C} U_{ij} = \zeta_C I_4, \quad (21)$$

with some phase factors $|\zeta_C| = 1$, as discussed in Section A.

Since $U_{ij}^2 = I_4$, not all the fluxes are independent. In the case of a \mathbb{Z}_2 gauge field, the constraints between multiple fluxes are called volume constraints [17]. However, due to the non-Abelian nature of the flux structure, it is subtle whether they apply. Fortunately, the above U^α ($\alpha = a, b, c$) obeys the following anticommutation relations.

$$\{U^\alpha, U^\beta\} = 2\delta^{\alpha\beta} I_4. \quad (22)$$

This algebraic relation proves the product of the fluxes of the loops surrounding some volume must vanish (volume constraints). Moreover, we can easily show that, if every bond color is used even times in each loop, which is a natural consequence for the lattices admitting materials realization, the flux inside should always be Abelian with $\zeta_C = \pm 1$. Actually, every lattice included in Table S1 obeys this condition, so we have already proven all of them have an Abelian flux sector.

The remaining subtle problem is which flux these elementary loops have, a zero flux, or a π flux. To check this, we need to investigate every loop one by one. To calculate every flux value systematically, we often use space group symmetries to relate two elementary loops, even though the system is in the strong spin-orbit coupling limit [20]. We have checked all the elementary loops in the tricoordinated lattices listed above [21]. Only the flux value for the shortest elementary loops is shown in Table S1.

* Also at Andronikashvili Institute of Physics, 0177 Tbilisi, Georgia.

- [1] D. P. Arovas and A. Auerbach, Phys. Rev. B **52**, 10114 (1995).
- [2] S. K. Pati, R. R. P. Singh, and D. I. Khomskii, Phys. Rev. Lett. **81**, 5406 (1998).
- [3] C. Itoi, S. Qin, and I. Affleck, Phys. Rev. B **61**, 6747 (2000).
- [4] K. I. Kugel, D. I. Khomskii, A. O. Sboychakov, and S. V. Streltsov, Phys. Rev. B **91**, 155125 (2015).
- [5] X. Chen, Z.-C. Gu, and X.-G. Wen, Phys. Rev. B **83**, 035107 (2011).
- [6] J. A. Watts, Inorg. Chem. **5**, 281 (1966).
- [7] W. Rüdorff, G. Walter, and H. Becker, Z. Anorg. Allg. Chem. **285**, 287 (1956).
- [8] T. Takayama, A. Kato, R. Dinnebier, J. Nuss, H. Kono, L. S. I. Veiga, G. Fabbri, D. Haskel, and H. Takagi, Phys. Rev. Lett. **114**, 077202 (2015).
- [9] K. A. Modic, T. E. Smidt, I. Kimchi, N. P. Breznay, A. Biffin, S. Choi, R. D. Johnson, R. Coldea, P. Watkins-Curry, G. T. McCandless, J. Y. Chan, F. Gandara, Z. Islam, A. Vishwanath, A. Shekhter, R. D. McDonald, and J. G. Analytis, Nat. Commun. **5**, 4203 (2014).
- [10] S. M. Winter, Y. Li, H. O. Jeschke, and R. Valentí, Phys. Rev. B **93**, 214431 (2016).
- [11] G. Jackeli and G. Khaliullin, Phys. Rev. Lett. **102**, 017205 (2009).
- [12] C. Wu, J.-p. Hu, and S.-c. Zhang, Phys. Rev. Lett. **91**, 186402 (2003).
- [13] C. Wu, Phys. Rev. Lett. **95**, 266404 (2005).
- [14] C. Wu, Mod. Phys. Lett. B **20**, 1707 (2006).
- [15] A. Georges, L. de' Medici, and J. Mravlje, Annu. Rev. Condens. Matter Phys. **4**, 137 (2013).
- [16] A. Kitaev, Ann. Phys. **321**, 2 (2006), January Special Issue.
- [17] K. O'Brien, M. Hermanns, and S. Trebst, Phys. Rev. B **93**, 085101 (2016).
- [18] O. Delgado Friedrichs, M. O'Keeffe, and O. M. Yaghi, Acta Crystallogr. Sect. A **59**, 22 (2003).
- [19] O. Delgado Friedrichs, M. O'Keeffe, and O. M. Yaghi, Acta Crystallogr. Sect. A **59**, 515 (2003).
- [20] The threefold rotation symmetry of the xyz -axes of the Cartesian coordinate is not clear in the gauge used in the main text. The spin quantization axis along the (111) direction will make this symmetry explicit.
- [21] M. G. Yamada, M. Oshikawa, and G. Jackeli, To be published.